THE FASEB JOURNAL
The Journal of the Federation of American Societies for Experimental Biology

RESEARCH ARTICLE

A novel BRET-Based GAP assay reveals phosphorylation-dependent regulation of the RAC-specific GTPase activating protein ARHGAP25

Éva Wisniewski[1] | Domonkos Czárán[1] | Fanni Kovács[1] | Enikő Bahurek[1] | Afrodité Németh[1] | Péter Sasvári[1] | Gergő Szanda[1] | Aladár Pettkó-Szandtner[2] | Eva Klement[2,3] | Erzsébet Ligeti[1] | Roland Csépányi-Kömi[1]

[1]Department of Physiology, Semmelweis University, Budapest, Hungary

[2]Laboratory of Proteomics Research, Biological Research Centre, Szeged, Hungary

[3]Single Cell Omics ACF, Hungarian Centre of Excellence for Molecular Medicine, Szeged, Hungary

Correspondence
Roland Csépányi-Kömi, Department of Physiology, Semmelweis University, Tűzoltó u. 37-47, Budapest 1094, Hungary.
Email: csepanyi-komi.roland@med.semmelweis-univ.hu

Abstract

ARHGAP25, a RAC-specific GTPase activating protein (GAP), is an essential regulator of phagocyte effector functions such as phagocytosis, superoxide production, and transendothelial migration. Furthermore, its complex role in tumor behavior has recently been recognized. We previously demonstrated that phosphorylation of serine 363 in ARHGAP25 regulates hematopoietic stem cells and progenitor cells in mouse bone marrow. However, the significance of other potential phosphorylation sites of ARHGAP25 remained unknown. Now, we developed a novel, real-time bioluminescence resonance energy transfer (BRET) assay to monitor the GAP activity of ARHGAP25 in vitro. Using this approach, we revealed that phosphorylation of S363 and S488, but not that of S379-380, controls ARHGAP25's RACGAP activity. On the other hand, we found in granulocyte-differentiated human PLB-985 cells that superoxide production and actin depolymerization are regulated by residues S363 and S379-380. The present data demonstrate the value of our BRET-GAP assay and show that different phosphorylation patterns regulate ARHGAP25's GAP activity and its effect on superoxide production and phagocytosis.

Abbreviations: BRET, bioluminescence resonance energy transfer; CRIB, CDC42- and RAC-interacting binding domain; DTT, dithiothreitol; GAP, GTPase activating protein; GDPβS, Guanosine 5′-[β-thio]diphosphate; GEF, Guanine nucleotide exchange factor; GST, glutathione-S-transferase; GTPγS, Guanosine 5′-[γ-thio]triphosphate; HPSC, hematopoietic stem cells and progenitor cell; IPTG, isopropyl 1-thio-β-d-galactopyranoside; LPP, Lambda protein phosphatase; MS, mass spectrometry; OPZ, opsonized zymosan; PH, pleckstrin homology; PKC, protein kinase C; PMA, phorbol 12-myristate 13-acetate; PMSF, phenylmethylsulfonyl fluoride; RLU, relative luminescence unit; TNFα, tumor necrosis factor alpha.

Éva Wisniewski and Domonkos Czárán should be considered joint first authors.

Journal Name	FSB2
Manuscript No.	22584
	WILEY
No. of pages: 19	Dispatch: 24-9-2022
PE:	CE:

1 | INTRODUCTION

Small GTPases of the Rho family (including RHO, RAC, and CDC42) are key components in actin cytoskeleton organization. Their downstream effectors regulate the polymerization and depolymerization of actin filaments, and the strict spatial and temporal coordination by Rho family small GTPases is crucial for normal cellular functions, for example, cell adhesion, migration, and immune cell responses, such as phagocytosis and superoxide production.[1–7] Rho GTPases act as molecular switches: GTP binding results in their active conformation stimulating downstream effectors. After slow, endogenous hydrolyzation of GTP, they turn to an inactive, GDP-bound state. Their cyclic operation is regulated by two types of proteins: guanine nucleotide exchange factors (GEFs) stimulate the dissociation of GDP, promoting the activation of small GTPases. GTPase activating proteins (GAPs) accelerate their slow GTP hydrolysis, which leads to the inactivation of the small GTPase, and finally, to signal termination.[8–12]

ARHGAP25, a GTPase activating protein, was first identified in 2004 in silico.[13] Later, our group was the first to investigate ARHGAP25 systematically, describe its tissue expression (mostly in leukocytes), RAC-specific activity and recognize its prominent role in phagocyte functions.[14–16] Additionally, in collaboration, we reported that phosphorylation occurs on serine 363 and may play a role in the mobilization of hematopoietic stem cells and progenitor cells (HPSCs) from murine bone marrow.[17] This previous study suggested multiple additional phospho-sites with hitherto unknown functions. Therefore, we aimed to systematically examine the possible role of these phospho-sites in leukocytes, the cell types with the highest ARHGAP25 expression. Recently, more and more papers report the involvement of ARHGAP25 in tumor migration and metastasis,[18–23] rendering the post-translational modifications of ARHGAP25 all the more relevant.

In this paper, we describe: (1) a new, real-time bioluminescence resonance energy transfer (BRET)-based in vitro method for measuring GTPase activity of phosphorylated wild type and mutant recombinant ARHGAP25 proteins; (2) besides S363, phosphorylation of the serine residue at position 488 is also involved in the regulation of RACGAP activity; (3) serine residue at position 379–380 has no direct effect on RAC's GTPase activity in vitro, however, it is essential to exert ARHGAP25's cellular effects in phagocytes.

2 | MATERIALS AND METHODS

2.1 | Reagents

Protease Inhibitor Cocktail, Phosphatase Inhibitor Cocktail 2, Phenylmethanesulfonyl-fluoride, adenosine 5′-triphosphate, Aprotinin, Leupeptin, Pepstatin A, Diisopropyl-fluorophosphate, Dithiothreitol, Guanosine 5′-diphosphate, Guanosine 5′-[β-thio]diphosphate, Guanosine 5′-[γ-thio]triphosphate, dimethylformamide, cytochrome c, phorbol myristate acetate, lucigenin, epidermal growth factor, zymosan, poly-L-lysine, Trypan Blue solution, Tween-20, and pGEX-4 T-1 vector were purchased from Sigma-Aldrich (St. Louis, MO, USA). One Shot™ BL21 Star™ Escherichia coli bacteria, Pierce™ Glutathione Agarose beads, Pro-Q™ Diamond Phosphoprotein Gel Stain, SYPRO™ Ruby Protein Gel Stain, CellTracker Green, and Alexa Fluor 568/488 conjugated phalloidin were from Invitrogen (ThermoFisher Scientific, Waltham, MA, USA). Dulbecco's modified Eagle medium with GlutaMAX I, UltraMEM, and RPMI-1640 media, as well as Amaxa Nucleofector™, were from Lonza (Basel, Switzerland). Hanks' Balanced Salt Solution (HBSS) was from HyClone (Logan, UT, USA). Lambda Protein Phosphatase was obtained from New England BioLabs (Ipswich, MA, USA), GTPase-Glo™ Assay and lipofectamine-HD was from Promega (Madison, WI, USA). Geneticin (G18) was purchased from Gibco (Invitrogen, Waltham, MA, USA). [γ-^{32}P]GTP was obtained from the Institute of Isotopes Co. Ltd. (Budapest, Hungary). CRIB-Rluc vector was a kind gift from András Balla, Cerulean-C1 and mVenus-N1 vectors were a gift from Péter Várnai.

2.2 | Cloning

Full-length human ARHGAP25 was cloned using cDNA from human peripheral blood as a template resulting in a 646 amino acid length protein. This protein corresponds to the Isoform 4 in the UniProt database (P42331-4) or the mRNA transcript variant 1 of the NCBI database (NM_001007231.2), which consists of an additional alanine at position 156 compared to the canonical sequence. It was cloned into pGEX-4 T-1, pcDNA3.1/V5-His-TOPO, and Cerulean C1 backbones. Full-length, GST-tagged recombinant ARHGAP25 was cloned

previously.[14] Additional mutations were introduced via site-directed mutagenesis using the primers indicated in Table S1. Mutations were confirmed by Sanger sequencing (Microsynth AG, Balgach, Switzerland). CRIB-Rluc was amplified and cloned into pGEX-4 T-1. RAC1 was also amplified and cloned into the mVenus-C1 backbone, and then into the pGEX-4 T-1 vector.

2.3 | Preparation of primary human neutrophilic granulocytes

Venous blood was drawn from healthy adult volunteers in accordance with the Declaration of Helsinki and approved by the National Public Health Center of Hungary (31937-7/2020/EÜIG). Neutrophilic granulocytes were prepared using dextran sedimentation followed by Ficoll-Paque gradient centrifugation as previously described.[24]

2.4 | Protein purification

Glutathione S-transferase (GST) fusion proteins were produced in One Shot™ BL21 Star™ Escherichia coli bacteria. Log-phase bacterial cells expressing GST-fusion proteins were induced with 0.5 mM isopropyl 1-thio-β-d-galactopyranoside (IPTG) at 37°C for 3 h. Bacterial pellets were lysed by sonication in a solution containing 50 mM Tris (pH 7.6), 50 mM NaCl, 5 mM $MgCl_2$, and 1 mM dithiothreitol (DTT), and before lysis, it was supplemented with 1 mM phenylmethylsulfonyl fluoride (PMSF), 1 mM Na-EGTA, 10 μg/ml aprotinin, 10 μM leupeptin, and 2 μM pepstatin A. After a centrifugation step at 8000 g for 20 min at 4°C, the supernatant was incubated with Pierce™ Glutathione Agarose beads for 30 min at 4°C and then washed three times. Samples on beads were stored at −80°C until further use. After preparation, the protein concentration was determined according to Bradford. Additionally, immediately before the experiment, protein concentrations were again checked and normalized using Nanodrop.

2.5 | Mass spectrometry

2.5.1 | Sample preparation

Primary human neutrophilic granulocytes or COS-7 cells were frozen in liquid nitrogen and ground in an Eppendorf tube with beads and sand. Total proteins from the cells were extracted as described.[25] Total protein extracts or recombinant protein samples were immunopurified using ARHGAP25 antibody and protein A-coupled magnetic beads with an average particle size of 50 nm (MACS® Technology, Bella Vista, New South Wales, Australia, Miltenyi) and digested in column with trypsin.[26] Alternatively, GST-tagged recombinant ARHGAP25 protein phosphorylated with a cytosolic extract from primary human neutrophils was digested in a solution with trypsin, the resulting tryptic peptide mixture desalted on a C18 ZipTip (Omix C18 100 μl tips, Varian) and subjected to Fe-NTA phosphopeptide enrichment.[27]

2.5.2 | Mass spectrometry analysis

An aliquot of the tryptic digest (with or without phosphopeptide enrichment) was analyzed by LC–MS/MS using a nanoflow RP-HPLC (Waters, LC program: linear-gradient of 3%–40% B in 30 or 100 min, solvent A: 0.1% formic acid in water, solvent B: 0.1% formic acid in acetonitrile) on-line coupled to an Orbitrap-Fusion™ Lumos (ThermoFisher Scientific, Waltham, MA, USA) mass spectrometer operating in positive ion mode. Data acquisition was carried out in a data-dependent fashion, the 20 most abundant, multiply charged ions were selected from each MS survey for MS/MS analysis using HCD fragmentation (both spectra were acquired in the Orbitrap).

2.5.3 | Data interpretation

The MS data presented in this study are openly available in FigShare at https://doi.org/10.6084/m9.figshare.19221312. Raw data were converted into peak lists using Proteome Discoverer (v 1.4) and searched against the UniProt Homo sapiens database (downloaded 2019.6.12, 172 251 proteins) using the Protein Prospector search engine (v5.15.1) with the following parameters: enzyme: trypsin with maximum two missed cleavage sites; mass accuracies: 5 ppm for precursor ions and 10 ppm for fragment ions (both monoisotopic); fixed modification: carbamidomethylation of Cys residues; variable modifications: acetylation of protein N-termini; Met oxidation; cyclization of N-terminal Gln residues, phosphorylation of Ser/Thr/Tyr, allowing maximum two variable modifications per peptide. Acceptance criteria: minimum scores: 22 and 15; maximum E values: 0.01 and 0.05 for protein and peptide identifications, respectively.

2.6 | Phosphorylation of recombinant GST-ARHGAP25

A total of 100 μg GST-tagged recombinant ARHGAP25 protein was phosphorylated with 150 μl of cytosolic

extract from primary human neutrophils (intact or heat-inactivated, in which case extracts were heated for 15 min at 100°C) (as previously described,[17]) in the presence of 30 μl kinase buffer (20 mM Tris–HCl, pH = 7.4, 10 mM $MgCl_2$, 0.1 mM Na-EGTA, 1 mM dithiothreitol (DTT), 1% Phosphatase Inhibitor Cocktail 2, 1% Protease Inhibitor Cocktail, 1 mM PMSF and 1 mM adenosine 5′-triphosphate (ATP) for 30 min on 30°C.

After washing three times in washing buffer (20 mM Tris–HCl, 5 mM KCl, 1.5 mM $MgCl_2$, and 1 mM DTT), GST-ARHGAP25 was eluted from Pierce™ Glutathione Agarose beads with a buffer containing 5 mM reduced glutathione.

Dephosphorylation was carried out using 400 U Lambda Protein Phosphatase in a total volume of 50 μl for 30 min at 30°C before elution.

2.7 | Staining of recombinant ARHGAP25 after phosphorylation

Recombinant ARHGAP25 proteins were run in SDS-PAGE gels, fixed, and stained with Pro-Q™ Diamond Phosphoprotein Gel Stain according to the manufacturer's instructions. Immediately after that, gels were stained with SYPRO™ Ruby Protein Gel Stain for the total protein amount. For imaging, we used a Typhoon 9410 (Amersham Biosciences, Amersham, United Kingdom) with a 532 nm excitation laser and a 560 nm long-pass filter for Pro-Q™ Diamond staining and 610 band-pass filters for SYPRO™ Ruby staining.

2.8 | GAP activity measurements

2.8.1 | In vitro bioluminescence resonance energy transfer (BRET)

Measurements were carried out on 96-well plates, in 100 μl/well total volume. Each well contained 2 μg GST-CRIB-Rluc (Renilla luciferase) dissolved in 20 mM Tris–HCl buffer (pH = 7.5), and 5 μg GST-Venus-RAC1. The fluorescence of the latter protein was also measured before each experiment to confirm that not only the concentration, but also the fluorescence intensity are identical between experiments. GST-Venus-RAC1 was preincubated ("loaded") beforehand with 30 μM GTP (or 0.3 mM GTPγS or GDPβS for positive and negative controls, resp.) for 10 min at room temperature in a low magnesium binding buffer (16 mM Tris–HCl, pH 7.5, 20 mM NaCl, 5 mM EDTA). Incubation of RAC was stopped, and GTP binding was stabilized by adding 25 mM $MgCl_2$ so that all the RAC proteins were in an active conformation. Then,

Renilla luciferase substrate coelenterazine h (5 μM) was added. Finally, the reaction was started by adding 15 μg GST-ARHGAP25 to the reaction as indicated in Table S2. The amount of GST-ARHGAP25 (μg/well) was optimized based on its dose–response curve on RAC's GTPase activity (Figure S3). Emissions were measured every 30 s for 15 min using 535–30 nm (Venus) and 475–30 nm (Rluc) filters at 25°C on a CLARIOStar luminometer (BMG Labtech, Ortenberg, Germany). Results were analyzed with MARS Data Analysis Software (BMG Labtech, Ortenberg, Germany). All BRET measurements were performed in duplicates, and BRET ratios were calculated by dividing the 535 nm and 475 nm intensities (Figure S2). BRET ratio of wells containing unloaded, GDP-bound GST-Venus-RAC1 and GST-CRIB-Rluc was used as background and subtracted from the stimulus-induced BRET ratios (Table S2). BRET ratio was displayed as the percentage of the 0 min value in each sample.

2.8.2 | GTPase-Glo™ assay

GTPase activity of different concentrations of ARHGAP25 was measured using the GAP-stimulated GTPase activity protocol of GTPase-Glo™ Assay. 2 μg GST-RAC was loaded with 1 μM GTP, and 0.5; 1; 5, and 10 μg recombinant ARHGAP25 was added in a final reaction volume of 25 μl on 96-well plates. Reactions were incubated for 30 min at room temperature. 25 μl GTPase Glo™ Reagent and later 50 μl Detection Reagent were added to the completed GTPase reactions according to the manufacturer's instructions. Luminescence (relative luminescence unit—RLU) was recorded using a CLARIOStar luminometer (BMG Labtech, Ortenberg, Germany) and represents the amount of remaining intact GTP in the assay. RLU was normalized to a positive control (PC) and was shown as a percentage. GTP without RAC or ARHGAP25 served as positive control, and RAC without GTP and ARHGAP25 as negative control (NC).

2.8.3 | Radioisotope assay

GST-RAC1 was loaded with [γ-^{32}P]GTP (more than 5000 Ci/mM) for 10 min at room temperature in low magnesium binding buffer (16 mM Tris–HCl, pH 7.5, 20 mM NaCl, 0.1 mM dithiothreitol [DTT], 5 mM EDTA, 100 nM [γ-^{32}P]GTP [5 μCi]). Then, 20 mM $MgCl_2$ was added (for 5 min on ice) to inhibit further nucleotide exchange. The reaction was started by adding [γ-^{32}P]GTP-loaded RAC to the assay buffer (16 mM Tris–HCl, pH 7.5, 0.1 mM DTT, 1 mg/ml bovine serum albumin, and 1 mM unlabeled GTP) containing unphosphorylated or phosphorylated GST-tagged recombinant

ARHGAP25. Samples were filtered through nitrocellulose membranes (0.45-µm pore size), followed by washing two times with 2 ml of cold buffer (50 mM Tris–HCl and 5 mM $MgCl_2$; pH 7.7). After the filters were dried, radioactivity was measured using a Beckman LS 5000TD liquid-scintillation spectrometer (Beckman Coulter, Brea, CA, USA).[14] GAP activity was shown as the decrease in RAC-bound ^{32}P[GTP] radioactivity retained on the filters (which is proportional to the active RAC amount).

2.9 | Cell lines and transfection

For our experiments, COS-7 (ATCC, Manassas, VA, USA) and PLB-985 (Leibniz Institute DSMZ, Braunschweig, Germany) cell lines were used. COS-7 cells were grown in Dulbecco's modified Eagle medium with GlutaMAX I, and PLB-985 cells were grown in RPMI-1640. Both media were supplemented with 10% (w/v) FBS, 50 units/ml penicillin, and 50 µg/ml streptomycin. Cells were grown in a 5% humidified CO_2 incubator at 37°C.

Transient transfection of COS-7 cells was performed with lipofectamine-HD following the manufacturer's instructions. Twenty-four hours before transfection, 70 000 cells were seeded on 25 mm coverslips (ThermoFisher Scientific: Waltham, Massachusetts, USA) in 6-well cell culture plates (JET Biofil, Guangzhou, China). Cells were transfected with phosphorylation-deficient mutant (S363A, S379-380A, S488A, S363A+S379-380A, S363A+S488A, S379-380A+S488A, triple mutant) variants of Cerulean-conjugated ARHGAP25 construct, wild type ARHGAP25-Cerulean, or the empty Cerulean-C1 vector.

PLB-985 cells were preincubated in UltraMEM medium without FBS or antibiotics for 1 h before transfection by Amaxa Nucleofector™ electroporation (following the manufacturer's instructions). PLB-985 cells were transfected with wild type-, the previously described phospho-deficient mutant ARHGAP25 constructs, and a plasmid containing the *LacZ* gene as control in a V5- and His-tagged plasmid (pcDNA3.1/V5-His-TOPO). This plasmid contains the neomycin antibiotic resistance gene enabling the selection of the transfected cells with the use of geneticin (G18). After transfection, cells were incubated in plain UltraMEM for 2 h, then the medium was changed to RPMI-985 supplemented with 10% (w/v) FBS, 50 units/ml penicillin, 50 µg/ml streptomycin, and 1 µg/ml geneticin. The cells were grown in this selective medium for at least 3 weeks before use. Expression levels of the different constructs were verified with Western blot analysis (Figure 6A).

Transfected PLB-985 cells were differentiated into neutrophil granulocytes for 7 days using 0.5% dimethylformamide.

2.10 | Immunoblotting

Transfected and differentiated PLB-985 cells were lysed in lysing buffer (30 mM Na-HEPES, 100 mM NaCl, 2% [w/v] Triton-X-100, 20 mM NaF, 1 mM Na-EGTA, 1 mM Na-EDTA, 100 mM benzamidine, 0.02% [w/v] diisopropyl-fluorophosphate, 1% [w/v] aprotinine, 1% [w/v] protease inhibitor cocktail, 1% [w/v] phosphatase inhibitor cocktail, and 1% [w/v] phenylmethylsulfonyl fluoride; pH 7.5) for 10 min on ice and centrifuged at 12 000 rpm for 10 min. The protein concentration of the supernatant was determined according to Bradford. Clear supernatants of the lysates were boiled at 100°C for 5 min in reducing SDS sample buffer and 40 µg protein of each sample was run on 4%–15% (w/v) gradient polyacrylamide gels (Bio-Rad, Hercules, California, USA). Separated proteins were then transferred to nitrocellulose membranes (Bio-Rad, Hercules, California, USA). After blocking for 15 min in EveryBlot blocking buffer (Bio-Rad, Hercules, California, USA), membranes were incubated with monoclonal anti-V5 antibody (Bio-Rad, Hercules, California, USA, MCA1360) in 1:1000 dilution overnight at 4°C. Bound antibody was detected with enhanced chemiluminescence using horseradish peroxidase-conjugated anti–mouse-Ig (from sheep) secondary antibody (GE Healthcare, Chicago, Illinois, USA, NA931V) in 1:5000 dilution (1 h, room temperature). GAPDH was detected with rabbit anti-GAPDH primary (1:5000 dilution) (Cell Signaling Technology: Danvers, Massachusetts, USA, #2118) and horseradish peroxidase-conjugated anti–rabbit-Ig secondary antibodies (1:5000 dilution) (GE Healthcare: Chicago, Illinois, USA, NA934V).

2.11 | Measurement of active RAC content using pull-down assay and western blotting

Transfected and differentiated PLB-985 cells were collected and divided into two subgroups: 3.5×10^6 cells were stimulated with 1.5 mg/ml opsonized zymosan (opsonization was performed with 10% pooled human serum at 37°C for 20 min) at 37°C for 30 min (OPZ), while the other half stayed on ice (not activated). All of them were lysed with lysis buffer containing 50 mM Tris–HCl, 100 mM $NaCl_2$, 2 mM $MgCl_2$, 10% (w/v) Glycerol, 1% Nonidet P-40 (Iqepal CA 630), 1% (w/v) aprotinine, 1% (w/v) Phosphatase Inhibitor Cocktail 2, 1% (w/v) Protease Inhibitor Cocktail and 1 mM PMSF for 5 min on ice, and after that the supernatant was separated from the insoluble debris by centrifugation (16 000 g, 5 min, 4°C). We performed a Bradford protein assay to determine the protein content and an equal amount of protein mass was loaded

into each well. We used a RAC-specific monoclonal antibody (BD Biosciences, NJ, USA, 610651) to determine the total RAC content and used GAPDH as a loading control (see 2.10. Immunoblotting). To obtain information about the active RAC content, we produced the appropriate GTPase-binding domain of p21-activated kinase (PAK-PBD) in a GST-tagged form (courtesy of Prof. T. Wieland) as described in section 2.4. Protein Purification. Cell lysates with an equal amount of protein mass were incubated with the beads for 50 mins at 5°C, then washed thrice and eluted in 1x Laemmli Sample Buffer at 95°C for 5 min. Equal volumes of each eluate were loaded for Western Blot, and we used RAC-specific monoclonal antibody to detect active RAC. We performed a densitometric analysis of the acquired x-ray films using the ImageJ software. First we calculated the RAC_{active}/RAC_{total} ratio and from these values, the change of active RAC ratio was determined between stimulated and non-stimulated cells ($\Delta RAC_{activated}/RAC_{total}$).

2.12 | Determination of ARHGAP25 membrane localization

COS-7 cells were transfected on coverslips as previously described. Forty-eight hours after transfection, cells were stimulated with 0.1 μg/ml epidermal growth factor (EGF) for 20 min in a 5% humidified CO_2 incubator at 37°C. After washing, cells were fixed with 4% paraformaldehyde, permeabilized with 0.1% (w/v) Triton-X 100, and F-actin was stained with Alexa fluor-568 conjugated phalloidin (ThermoFisher Scientific, Waltham, Massachusetts, USA, A12380). Between each step, cells were washed four times with phosphate-buffered saline (PBS). Images were captured using a Zeiss LSM510 laser scanning confocal microscope equipped with a 63x/1.3 oil immersion objective (Plan-Neofluar, Zeiss, Oberkochen, Germany) and analyzed with LSM Image Browser software (Zeiss, Oberkochen, Germany). In each experiment 100–100 transfected cells were inspected by three investigators in a blinded set-up to determine the ratio of cells displaying ARHGAP25 localization to the membrane.

2.13 | Measurement of filamentous actin

Two million transfected and differentiated PLB-985 cells were fixed with 4% paraformaldehyde for 15 min at room temperature and permeabilized with PBS containing 0.1% Tween-20 for 5 min at room temperature. F-actin was stained using Alexa fluor-488 conjugated phalloidin (ThermoFisher scientific: Waltham, Massachusetts, USA, A1279), in 1:100 dilution for 20 min at room temperature.

Between every step, cells were washed four times with PBS. The mean fluorescence of 10 000 cells was measured in each sample with a Cytoflex flow cytometer (Beckman Coulter, Brea, California). For visualization of F-actin, coverslips were coated with 100 μg/ml poly-L-lysine overnight, then transfected and differentiated PLB-985 cells were seeded on them for 2 h. Cells were fixed using 4% paraformaldehyde (15 min), permeabilized with 0.1% Tween-20 (5 min), and stained with Alexa-488 conjugated phalloidin (20 min) on the coverslips. Between each step, samples were washed three times with PBS. Images were captured using a Zeiss LSM510 laser scanning confocal microscope equipped with a 63x/1.3 oil immersion objective (Figure S6).

2.14 | Measurement of phagocytosis

Yeast cells were boiled at 95°C for 30 min, then fluorescently stained with 2 μM of CellTracker Green and opsonized with 10% pooled human serum for 30 min at 37°C. After washing the yeast cells three times with HBSS, 5×10^5 transfected and differentiated PLB-985 cells were incubated with 5×10^6 yeast cells for 5 min at 37°C in HBSS, and then cells were fixed using 4% paraformaldehyde. The fluorescence of bound, but not engulfed yeast cells was quenched using 0.5% Trypan Blue solution. The ratio of phagocyting cells was determined using a Cytoflex flow cytometer by measuring 10 000 cells/sample.

2.15 | Measurement of superoxide production

PLB-985 cells were transfected and differentiated into neutrophil granulocytes as previously described.

For the measurement of extracellular superoxide production, cells were mixed with 100 μM cytochrome c and stimulated with 100 nM phorbol myristate acetate (PMA) on a 96-well flat-bottom plate (Greiner, Frickenhausen, Germany) (2×10^5 cells/well) in Hanks' Balanced Salt Solution (HBSS). Changes in OD were followed for 30 min on 550 and 450 nm wavelength and the difference in OD was calculated (normalization of the maximal absorbance wavelength of cytochrome c to its minimal absorbance wavelength). Background OD was measured without PMA for each transfected cell type and was subtracted from the stimulated values.

Intracellular superoxide production was determined by lucigenin luminescence. 50 μg/ml lucigenin was added to the cells and 2×10^6 cells were stimulated with 1.5 mg/ml opsonized zymosan (opsonization was performed with 10% pooled human serum at 37°C for 20 min) in each well on a

96-well, white, flat bottom plate (Greiner, Frickenhausen, Germany) in HBSS buffer. Luminescence was measured for 1 h on 450–550 nm spectra on a CLARIOstar luminometer (BMG Labtech, Ortenberg, Germany). Background luminescence was measured without opsonized zymosan for each transfected cell type.

2.16 | Statistical analysis

All data were analyzed and plotted using GraphPad Prism 8.0.1 Software. Pairwise comparison of experimental groups was carried out with paired *t*-test, one-way ANOVA, or two-way ANOVA followed by a Tukey post hoc test, depending on the condition. All *p* values <.05 were considered statistically significant.

3 | RESULTS

3.1 | Development of a bioluminescence resonance energy transfer (BRET)-based method for measuring the GAP activity of ARHGAP25

In our previous study, in silico analysis and investigation of the truncated fragments of ARHGAP25 revealed that the interdomain region of ARHGAP25 (from amino acid residue 355 to 541) is the primary target for phosphorylation.

Mass spectrometry data strongly suggested the functional importance of phosphorylation of S363, S379, and S488.[17] Later, we performed several mass spectrometry analyses on four different sample types: recombinant protein, COS-7 cells transfected with ARHGAP25, differentiated PLB-985 cells, and human neutrophilic granulocytes, the latter two containing endogenous ARHGAP25 (for raw data, see: https://doi.org/10.6084/m9.figshare.19221312). In these analyses, we found several phosphorylated residues, among which we confirmed the phosphorylation of S363, S379-380, and S488 (Figure S1). We also uploaded an Excel file to figshare to summarize our MS findings and a Venn diagram showing the most often phosphorylated residues within ARHGAP25 (https://doi.org/10.6084/m9.figshare.19221312). Since mass spectrometry is unable to differentiate between phosphorylation of the neighboring serine residues 379 and 380, we referred to them as one entity in terms of phosphorylation (S379-380) (Figure 1A).

To investigate whether these modifications play any role in the regulation of ARHGAP25's RACGAP activity, we sought a straightforward GAP assay. However, available methods to monitor GAP activity either provide end-point read-outs only or are highly labor-intensive and expensive. These limitations prompted us to develop a new, in vitro bioluminescence-resonance energy transfer (BRET)-based method. First, we generated GST-tagged, recombinant RAC fused with Venus fluorescent protein. GST-tagged CDC42- and RAC-interacting binding domain (CRIB) was also cloned and linked with *Renilla* luciferase
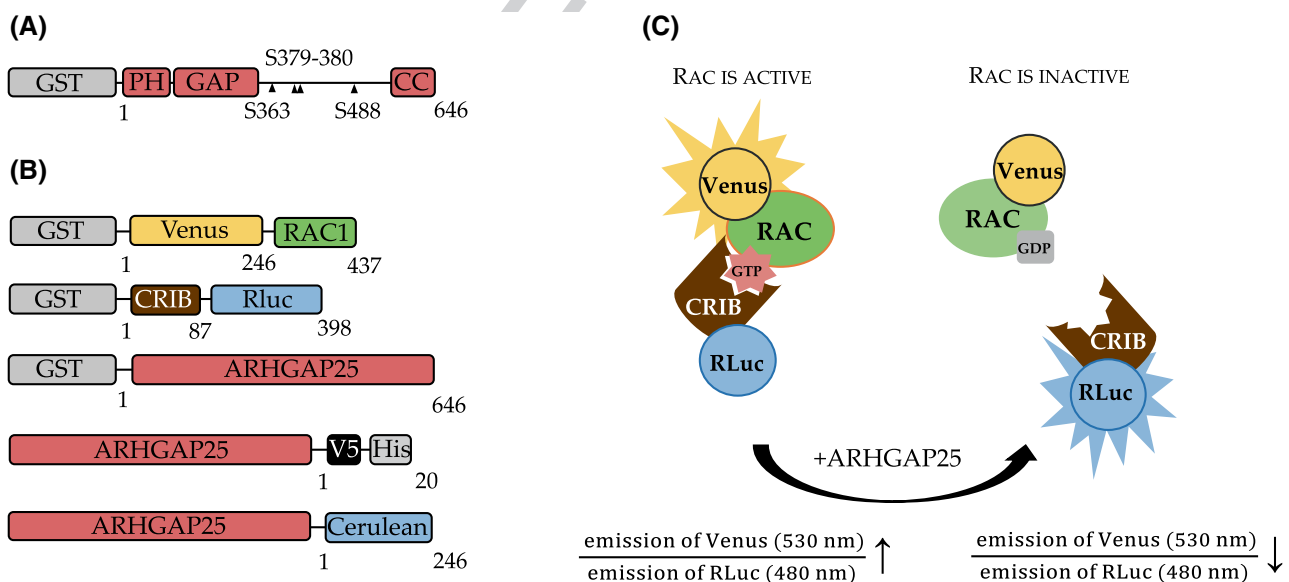

FIGURE 1 ARHGAP25 constructs and schematic representation of the BRET-based GAP assay. (A) ARHGAP25 consists of a pleckstrin homology (PH) domain, a GTPase activating (GAP) domain and a coiled-coil region (CC) at the C-terminus. The assumed serins involved in phosphorylation are S363, S379-380 and S488; (B) In the BRET-based GAP assay ARHGAP25, Venus-tagged RAC and Renilla luciferase-tagged CRIB (CRIB-RLuc) were expressed as GST-fusion proteins. For in vivo experiments, V5-tagged and Cerulean-tagged ARHGAP25 constructs were created; (C) shows the schematic representation of our BRET-based GAP assay. CRIB, Cdc42- and RAC-interactive binding domain; GST, glutathione-S-transferase.

(RLuc) (Figure 1B). CRIB binds RAC only in its GTP-bound, active conformation, resulting in the molecular proximity of Venus and RLuc. With the addition of its substrate, coelenterazine, the latter excites Venus by energy transfer causing an increase in the so-called BRET ratio, which equals the emission of Venus (530 nm) divided by the emission of RLuc (480 nm). After hydrolyzation of GTP, RAC turns to an inactive, GDP-bound form and releases CRIB, terminating the energy transfer between RLuc and Venus, and thereby decreasing the BRET ratio. Therefore, the active amount of RAC is proportional to the BRET ratio. Supplementing the mixture with recombinant ARHGAP25, its RACGAP activity is seen as a decrease in the BRET ratio (Figure 1C).

First, we validated our BRET-based GAP assay by demonstrating the RACGAP activity of wild type ARHGAP25. In real-time experiments, endogenous GTP hydrolysis of RAC was displayed as a slight decrease in BRET ratio, which differed from the positive control sample, in which RAC was loaded with the non-hydrolyzable GTP analog GTPγS (Figure 2A). The addition of wild type recombinant ARHGAP25 remarkably accelerated the endogenous GTP hydrolysis of RAC similarly to that observed with the radioisotope-based method (Figure 2A,B). Notably, the effect of ARHGAP25 on the BRET ratio proved to be dose dependent (Figure 2C).

As a next step, we wished to compare the dose dependency of our BRET-based method to the classical radioisotope-based method (Figure 2D) and the GTPase-Glo™ assay (Figure 2E). BRET results were comparable to those obtained with these established experimental procedures, however, we attained higher sensitivity with generally less variance with our method. Taken together, we showed that this novel approach is a reliable method to monitor ARHGAP25's GAP activity in a real-time manner.

3.2 | BRET-based GAP assay is suitable for the detection of phosphorylation-dependent RACGAP activity of ARHGAP25

Next, we investigated whether our BRET-based assay is suitable for detecting the negative effect of phosphorylation on ARHGAP25's RACGAP activity, which was partially described previously.[17] Recombinant ARHGAP25 was phosphorylated by neutrophilic cytosol extract, and samples were separated on SDS polyacrylamide gel. Phosphorylation was tested with Pro-Q™ Diamond Phosphoprotein Gel Staining (Figure 3A). As expected from previous data,[17] neutrophilic cytosol caused remarkable phosphorylation of ARHGAP25 compared to the control sample, where no cytosol treatment was carried out. Heat inactivation of the cytosol completely abolished the

phosphorylation signal, as did the treatment of the samples with lambda phosphatase (Figure 3A). To test the effect of phosphorylation, we compared the previously applied radioisotope-based assay and our BRET-based method. In end-point measurements both assays showed very similar results: non-phosphorylated ARHGAP25 significantly reduced the active RAC amount by its relatively high GTPase activating effect. In contrast, phosphorylated ARHGAP25 was less active as a GAP (Figure 3B).

To further strengthen the notion that phosphorylation alone is the mediator of reducing ARHGAP25's GAP activity, we used lambda protein phosphatase (LPP) treatment. Eliminating the phosphate groups in ARHGAP25 fully restored its GAP activity (Figure 3C).

To exclude the possibility that the observed changes are due to other cytosolic factors and not phosphorylation, we generated a GAP-dead mutant ARHGAP25 construct, as previously described.[14] This mutant showed a significantly impaired GAP activity which was independent from the cytosol treatment (Figure 3D).

3.3 | Phosphorylation of S363 or S488, but not of S379-380 mitigates the RACGAP activity of ARHGAP25

Now taking advantage of our BRET-based GAP assay, we started to study the role of phosphorylation on the above-mentioned serine residues. Therefore, we mutated them individually or in pairs to alanine (S-A mutants), and the mutants' GAP activity was measured after phosphorylation with intact (ARHGAP25-P) or heat-inactivated cytosol (ARHGAP25). When incubating the samples with buffer only (no cytosol), the curves did not differ from the HI cytosol-treated ones (Figure S4). Nevertheless, the latter contains all cytosolic proteins and fragments with inactive enzymes, therefore we chose the HI cytosol-treatment as a non-phosphorylated control in the following experiments. In this set of experiments, S363A was used as a reference, because the inhibitory effect of phosphorylation on this residue was shown earlier.[17] It is important to note that our in vitro BRET assay was conceived to measure differences between the phosphorylated and unphosphorylated form of the same mutant and not to make comparisons between mutants.

Mutation of S363 to alanine (Figure 4B) completely abolished the inhibitory effect of phosphorylation on ARHGAP25's RACGAP activity compared to WT (Figure 4A), similarly to that observed previously using the radioisotope-based method.[17] S488A mutant acted similarly to S363A: RACGAP activity did not differ from the non-phosphorylated form after neutrophil cytosol treatment (Figure 4D), suggesting that phosphorylation of these two residues is necessary for the inhibitory effect on ARHGAP25's
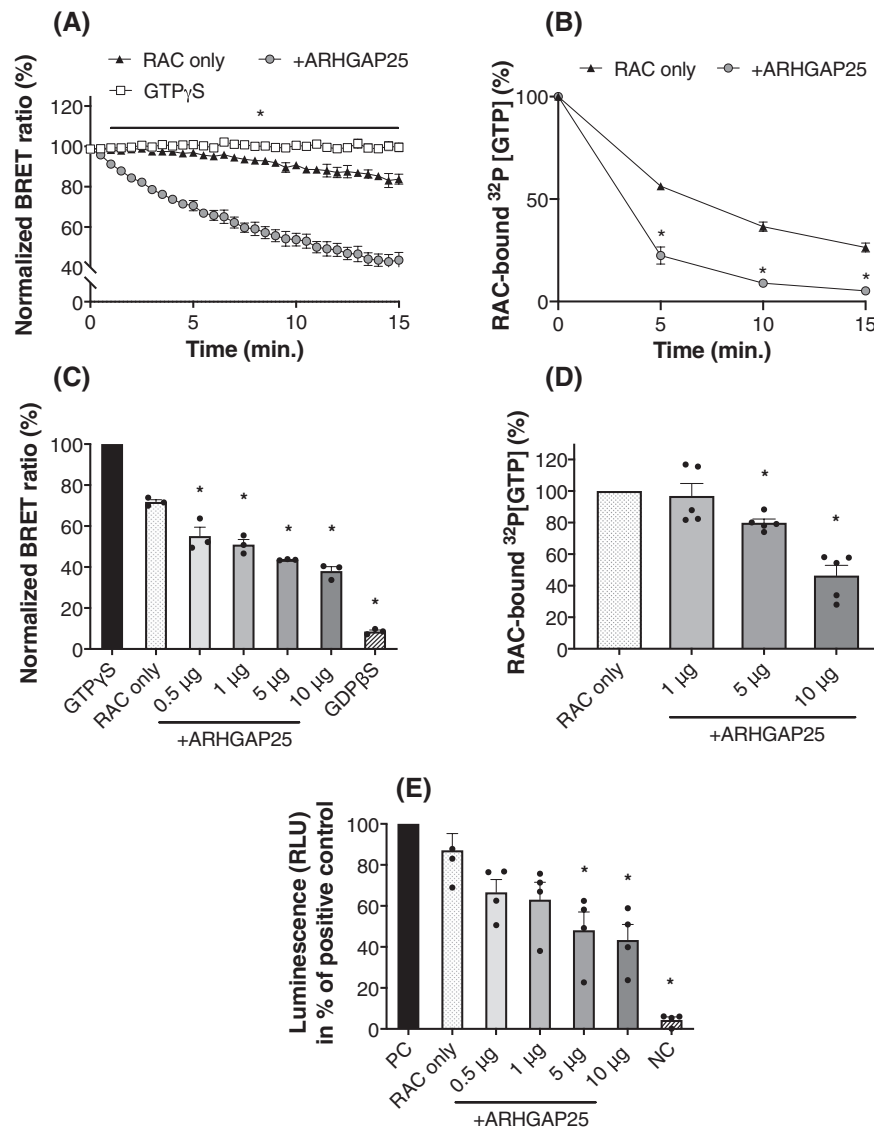
FIGURE 2 The in vitro BRET-based GAP assay is comparable to other known GAP assays. (A) Wild type ARHGAP25 enhances RAC's poor endogenous GTPase activity which is shown as a more profound fall in normalized BRET ratio %. Loading RAC with GTPγS instead of GTP prevents the dissociation of RAC and CRIB, showing the maximal normalized BRET ratio %. Mean ± SEM of 4 independent experiments. Significance is shown in a from-to interval, *$p < .05$ ARHGAP25 compared to RAC based on two-way ANOVA with Tukey post-hoc test; (B) radioisotope GAP assay shows ARHGAP25's GAP activity as a decrease in isotope-labeled GTP. Mean ± SEM of 5 independent experiments, *$p < .05$ ARHGAP25 compared to RAC after two-way ANOVA; (C) BRET-based GAP assay; (D) radioisotope GAP assay; and (E) GTPase-Glo™ Assay shows the dose dependency of ARHGAP25's GTPase activating effect where the indicated amount of ARHGAP25 was added to RAC. Mean + SEM of three (C and E) and five (D) independent experiments are plotted. *$p < .05$ ARHGAP25 compared to RAC using one-way ANOVA analysis. NC, negative control; PC, positive control.

RACGAP activity. Interestingly, mutation of serine residues at positions 379 and 380 (S379-380A) showed an altered phenotype compared to the previous mutants: phosphorylation caused a significant inhibition of ARHGAP25's RACGAP activity comparable to the wild type protein (Figure 4A,C).

Investigation of the double-mutant proteins painted a more nuanced picture of their role. Double S-A mutation of serine residues S363 and S488 showed no inhibitory effect after phosphorylation (Figure 4F), similarly to the S379-380A + S488A construct (Figure 4G). Phosphorylation of S363A + S379-380A

mutant ARHGAP25 caused a slight decrease in RACGAP activity (Figure 4E). Surprisingly, phosphorylation of the triple mutant ARHGAP25 (S363A + S379-380A + S488A) decreased its RACGAP activity compared to the single mutants S363A and S488A (Figure 4H). These observations suggest that mutations of S379 and/or S380 may have a more specialized effect and are not directly involved in inhibiting ARHGAP25's RACGAP activity by phosphorylation. For better comparison, we calculated decay rates from normalized BRET ratio data by fitting regression lines on the initial 2-min linear section of the
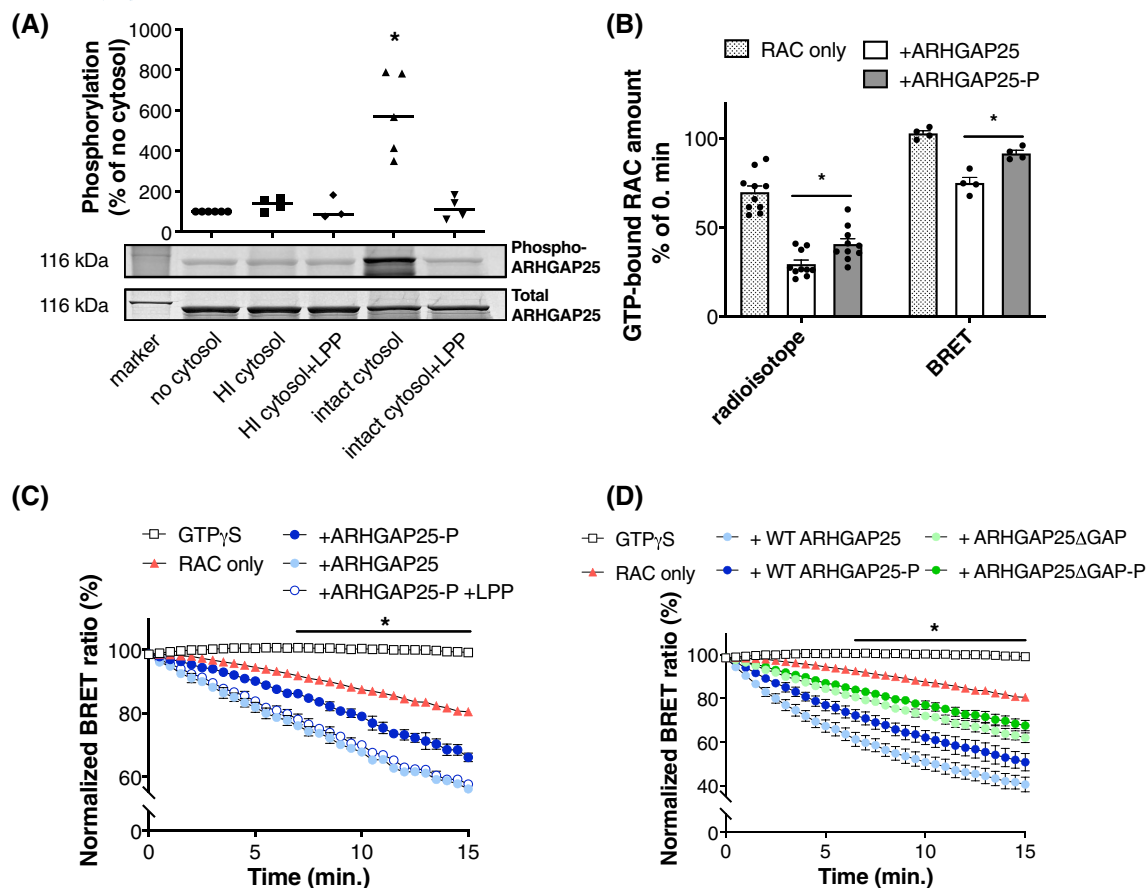
THE **FASEB** JOURNAL

FIGURE 3 Phosphorylation-dependent change in RACGAP activity of ARHGAP25 is appropriately measurable by BRET-based GAP assay. (A) Recombinant ARHGAP25 was incubated with neutrophilic cytosol and stained in gel with Pro-Q™ Diamond Phosphoprotein Gel Stain for phosphoproteins and later with SYPRO™ Ruby Protein Gel Stain for total protein. The phosphoprotein/total protein ratio is shown as the percentage of non-treated ARHGAP25. Treatment with intact cytosol causes dominant phosphorylation compared to heat-inactivated (HI) cytosol, which is reversed by lambda phosphatase (LPP) treatment. *$p < .05$ intact cytosol treatment compared to no cytosol using one-way ANOVA; (B) Five minutes after adding ARHGAP25 to the reaction, non-phosphorylated ARHGAP25 (+ARHGAP25) decreases RAC's endogenous GTPase activity (RAC only), while phosphorylated ARHGAP25 (+ARHGAP25-P) has only a reduced GAP activity represented by both a radioisotope and BRET-based GAP assay, *$p < .05$ ARHGAP25-P compared to ARHGAP25, calculated with two-way ANOVA. Mean + SEM of four (BRET) or ten (radioisotope) biological replicates are shown; (C) Phosphorylation of ARHGAP25 weakens its GAP activity, which effect can be reversed with lambda phosphatase (LPP) treatment. '+ARHGAP25' corresponds to the protein incubated with heat-inactivated cytosol. *$p < .05$ ARHGAP25-P compared to ARHGAP25-P + LPP, calculated with two-way ANOVA with Tukey post-hoc test. Mean ± SEM of three independent experiments are shown; (D) Unlike the wild type protein, GAP-dead ARHGAP25 shows a weakened GAP activity regardless of the phosphorylation state. Mean ± SEM of three independent experiments are shown. *$p < .05$ WT ARHGAP25-P compared to WT ARHGAP25 using two-way ANOVA.

curves. We found the same significant changes between phosphorylated and non-phosphorylated forms of ARHGAP25 mutants as in the kinetic measurements (Figure 4I).

3.4 | Plasma membrane binding of ARHGAP25 is independent of the single phosphorylation of S363, S488, and/or S379-380

With its pleckstrin homology (PH) domain, ARHGAP25 can bind phospholipids.[14,28] To test whether the currently studied

serine residues have any role in regulating ARHGAP25's lipid binding, we examined the plasma membrane localization of the protein in transfected COS-7 cells. We chose COS-7 cells due to their phenotype which enables a better visualization of subcellular localization. In order to activate RAC in these cells, we stimulated them with EGF, for it was published earlier that epidermal growth factor (EGF) initiates Akt/mTOR pathway as well as membrane ruffling through RAC, and ARHGAP25 is involved in both processes.[14,22,29,30] Cerulean-C1 vector alone mainly localized in the nucleus of the cells and a minor cytoplasmic localization was also observed. In contrast, we found that overexpressed
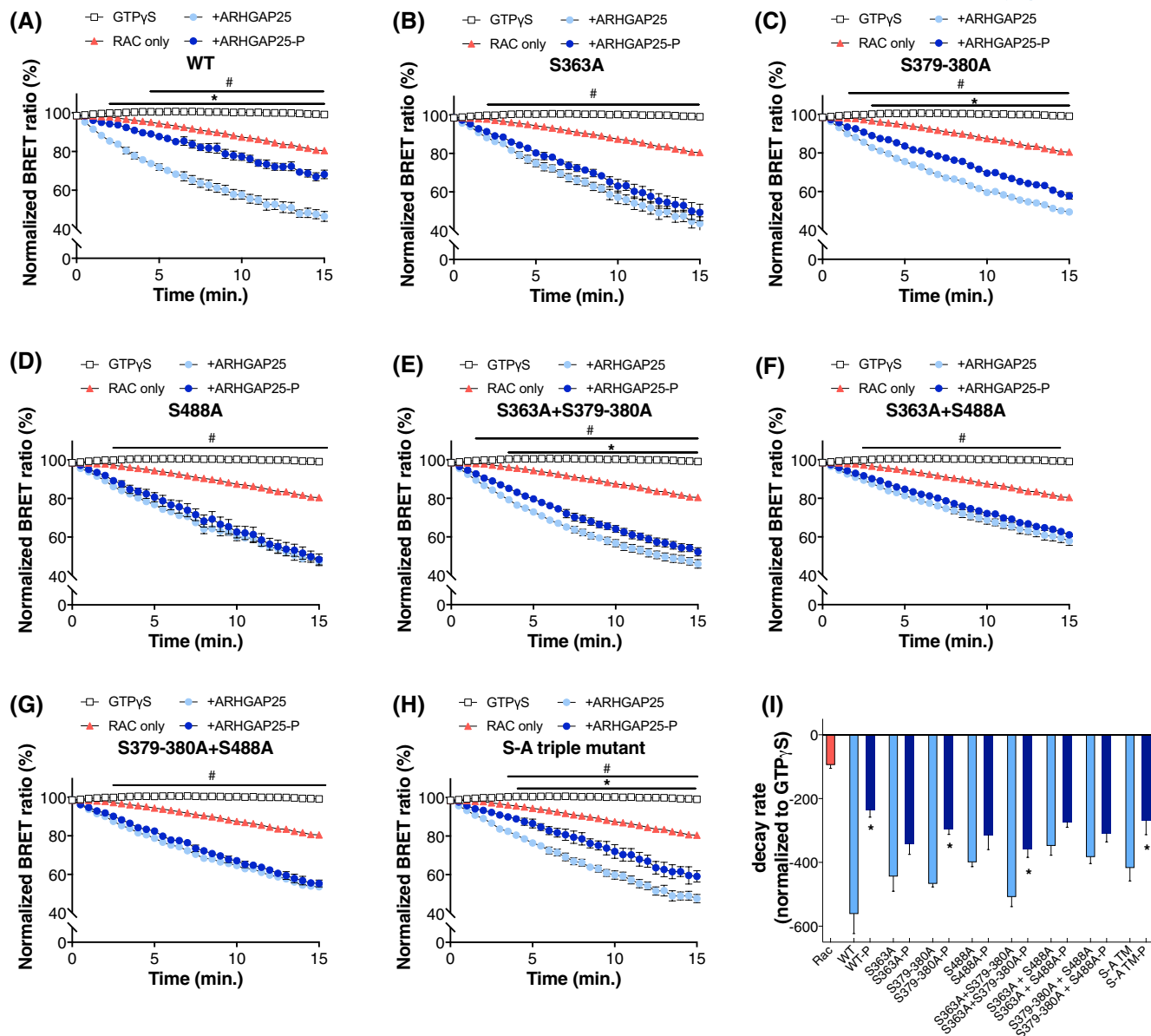
FIGURE 4 Effect of phosphorylation-deficient (Ser-to-Ala) mutations on the GAP activity of ARHGAP25. (A–I) Wild type and mutant recombinant ARHGAP25 constructs were pre-treated with neutrophil cytosol (intact or heat-inactivated, referred to as ARHGAP25-P and ARHGAP25, resp.) for 30 min and then added to Venus-RAC and CRIB-Rluc. Mean ± SEM of four (A, D, F, G, and H), five (B and C), or eight (E) independent experiments were plotted. Regarding RAC and GTPγS, the mean ± SEM of 50 independent experiments (biological replicates) is shown. The lines above the diagrams show the significance of a from-to-interval. Data were analyzed using two-way ANOVA followed by a Tukey post hoc test. $^{\#}p < .05$ ARHGAP25-P compared to RAC, $*p < .05$ ARHGAP25-P compared to ARHGAP25; (I) Decay rate in the first 2 min of panels A-H was calculated and plotted (normalized to GTPγS). $*p < .05$ ARHGAP25-P compared to ARHGAP25 based on unpaired t-tests.

ARHGAP25 constructs were visible both in the cytosol and at the plasma membrane. To evaluate the confocal microscopic images, 100 transfected cells were counted in each experiment, and the percentage of cells showing apparent plasma membrane localization was determined. According to our results, single or double mutation of the indicated serine residues did not affect the plasma membrane localization of ARHGAP25, however, the triple mutant showed altered localization (Figure 5A,B; Figure S5).

3.5 | Phosphorylation of S379 and/or S380 residues of ARHGAP25 are key components of the regulation of actin-reorganization

As we reported previously, ARHGAP25 is highly expressed in leukocytes and has a key role in regulating elementary phagocyte functions.[14,31] Since COS-7 cells are not able to perform leukocyte functions such as phagocytosis or
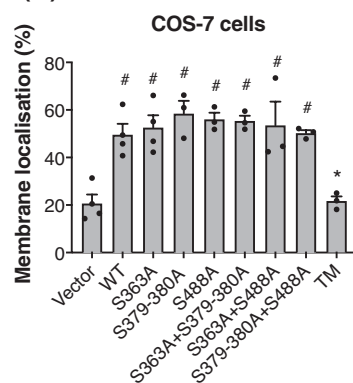
(A)
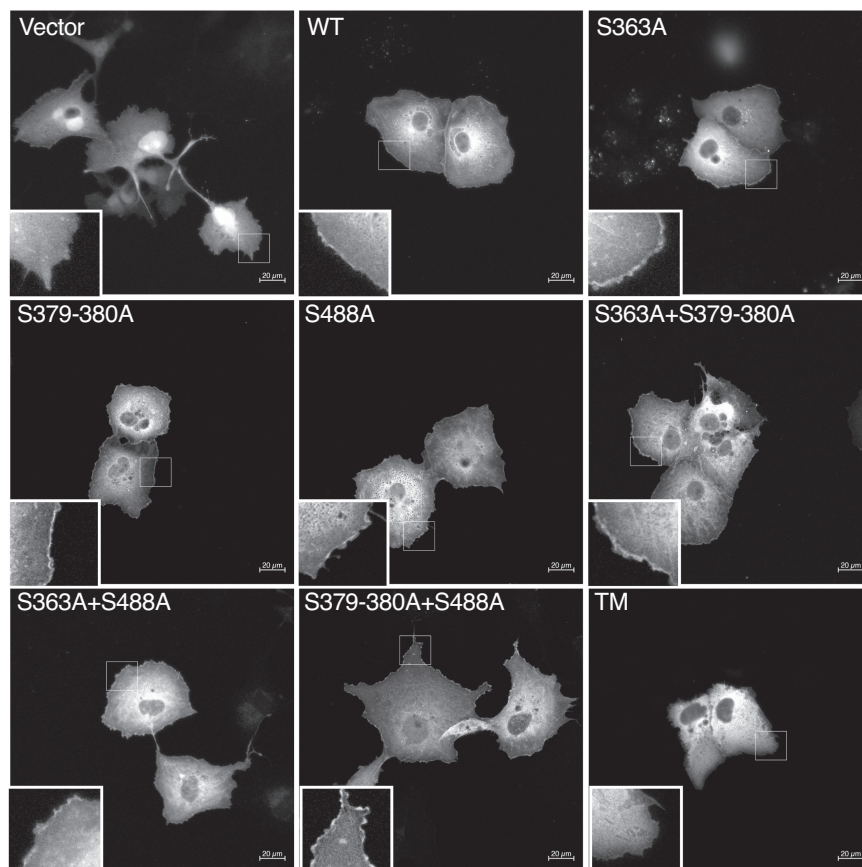
FIGURE 5 Plasma membrane localization of ARHGAP25 in COS-7 cells. (A) COS-7 cells were transfected with Cerulean-C1 conjugated forms of the indicated ARHGAP25 constructs and stimulated with EGF for 20 min. Hundred transfected cells were examined in each independent experiment. Representative pictures of the localization of ARHGAP25 to the plasma membrane are shown. Inserts show the enlarged parts of the cells indicated by rectangles. F-Actin staining is shown in Figure S4. Plasma membrane localization was observed in case of transfection with WT and all single and double mutant constructs, but not that of empty Cer-C1 vector and S-A triple mutant-transfected cells; (B) Percentage of cells, where the localization of ARHGAP25 to the plasma membrane was clearly visible, was calculated;

(B)

superoxide production, we decided to use the PLB-985 acute human myeloid leukemia cell line. After stable transfection with V5-tagged ARHGAP25 S-A mutant or wild type (WT) constructs, cells were differentiated into neutrophilic granulocytes. Expression levels were analyzed with a V5-specific antibody in Western blot. No significant difference was observed in the expression or integrity of the constructs. Regarding the vector, a higher band (approx. 120 kDa) was detected, which corresponds to V5-tagged β-galactosidase (Figure 6A).

It is known that ARHGAP25 regulates actin-polymerization/depolymerization through RAC, and filamentary actin is also required for normal superoxide production of neutrophils.[14,15,28] Following this line, we investigated the F-actin amount of resting, stably transfected PLB-985 cells differentiated into neutrophils. Overexpression of wild type ARHGAP25 significantly reduced the amount of F-actin compared to the control vector (Figure 6B). Single mutants S363A or S488A were functionally identical to WT in this aspect (Figure 6B).

(A) PLB-985 cells
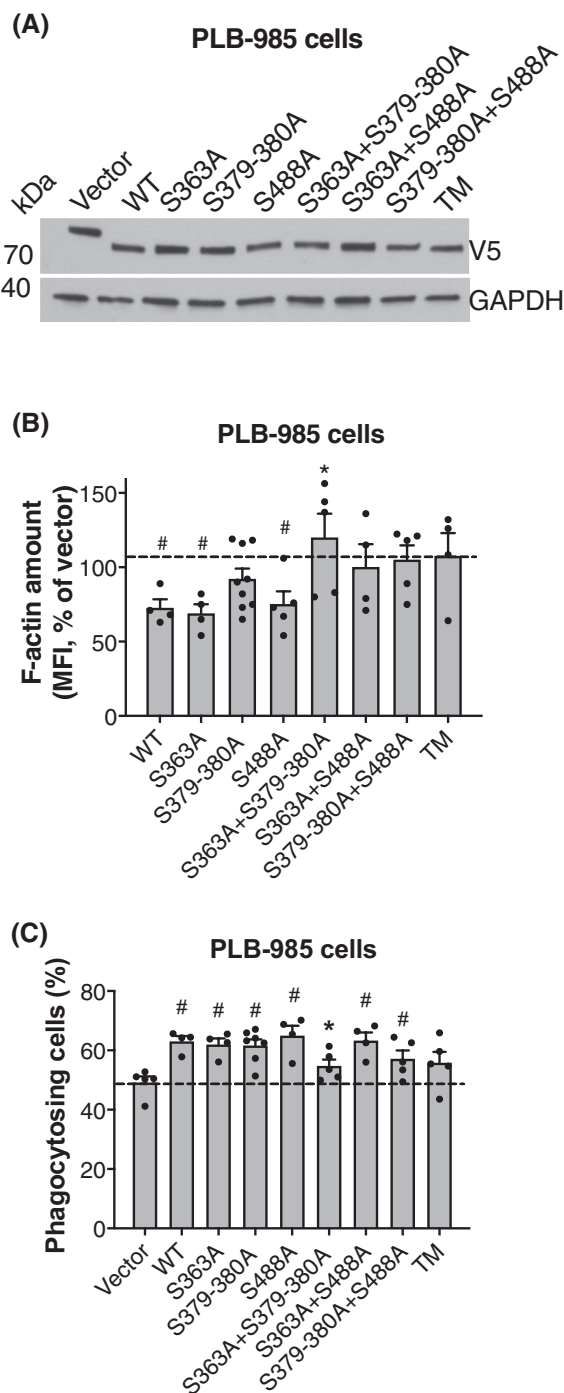
(B) PLB-985 cells

(C) PLB-985 cells

FIGURE 6 Filamentous Actin (F-Actin) content and phagocytosis of PLB-985 cells transfected with different ARHGAP25 S-A mutant constructs. (A) PLB-985 cells were transfected with the indicated V5 tagged constructs of ARHGAP25 or the vector containing the *LacZ* gene as a control. Cells were grown in a selective medium containing geneticin for 3 weeks and differentiated into neutrophils. Cell lysates were separated with SDS gel electrophoresis, and Western blot analysis was performed using a V5 tag-specific antibody. As a loading control, GAPDH was used. (B) F-actin in transfected and differentiated PLB cells was stained using fluorescently labeled phalloidin after fixing the cells with 4% paraformaldehyde and permeabilizing them with 0.1% Tween-20. The mean fluorescence intensity of 10 000 cells was measured using flow cytometry in each experiment. Mean + SEM of four (WT, S363A, S363A + S488A, TM) or five (Vector, S379-380A, S363A + S379-380A, S379-380A + S488A, TM) independent experiments were shown; (C) Phagocytosis of PLB-985 cells transfected with different ARHGAP25 S-A constructs. Transfected and differentiated PLB cells were incubated for 5 min at 37°C with fluorescently labeled, and pooled serum opsonized yeast cells, then fixed with 4% paraformaldehyde. The ratio of phagocyting cells was determined using flow cytometry. Mean + SEM of four independent experiments. Data were analyzed using one-way ANOVA followed by a Tukey post hoc test. #$p < .05$ compared to vector. *$p < .05$ compared to WT.

3.6 | Phosphosite mutant S363A + S379-380A mitigates the phagocytic activity of PLB-985 cells

Phagocytosis of large particles depends on actin reorganization, and the latter is regulated by ARHGAP25.[14,28] We decided to investigate this process through the phagocytosis of yeast particles in PLB-985 neutrophilic cell line. Overexpression of WT ARHGAP25 resulted in a higher phagocytic rate compared to control. Phosphosite mutations showed similar phagocytic activity; only the S363A + S379-380A mutant could significantly reduce the above parameter compared to WT (Figure 6C).

3.7 | S379-380 are essential for regulating superoxide production in PLB-985 human neutrophilic cell line

Next, we decided to investigate the superoxide production of neutrophilic granulocytes, a function in which the specific regulatory role of ARHGAP25 was already confirmed.[14,16] Superoxide production was induced with phorbol 12-myristate 13-acetate (PMA) (Figure 7) or with pooled human serum opsonized zymosan (Figure 8). As expected, overexpression of WT ARHGAP25 inhibited the superoxide production compared to control, independently of the stimulus (Figures 7 and 8).

On the other hand, defective phosphorylation of S379-380 almost eliminated the actin-depolymerizing effect of ARHGAP25, while overexpression of the double mutant S363A + S379-380A resulted in a higher f-actin amount than we observed with the control vector-transfected cells (Figure 6B). The other double mutants containing S488A and the triple mutant, did not affect the F-actin amount compared to the control vector (Figure 6B). Microscopic slides were also prepared for visualization, and images were captured with confocal microscopy (Figure S6). These data suggest that serine residues at positions 379 and/or 380 play a crucial role in regulating actin-reorganization.
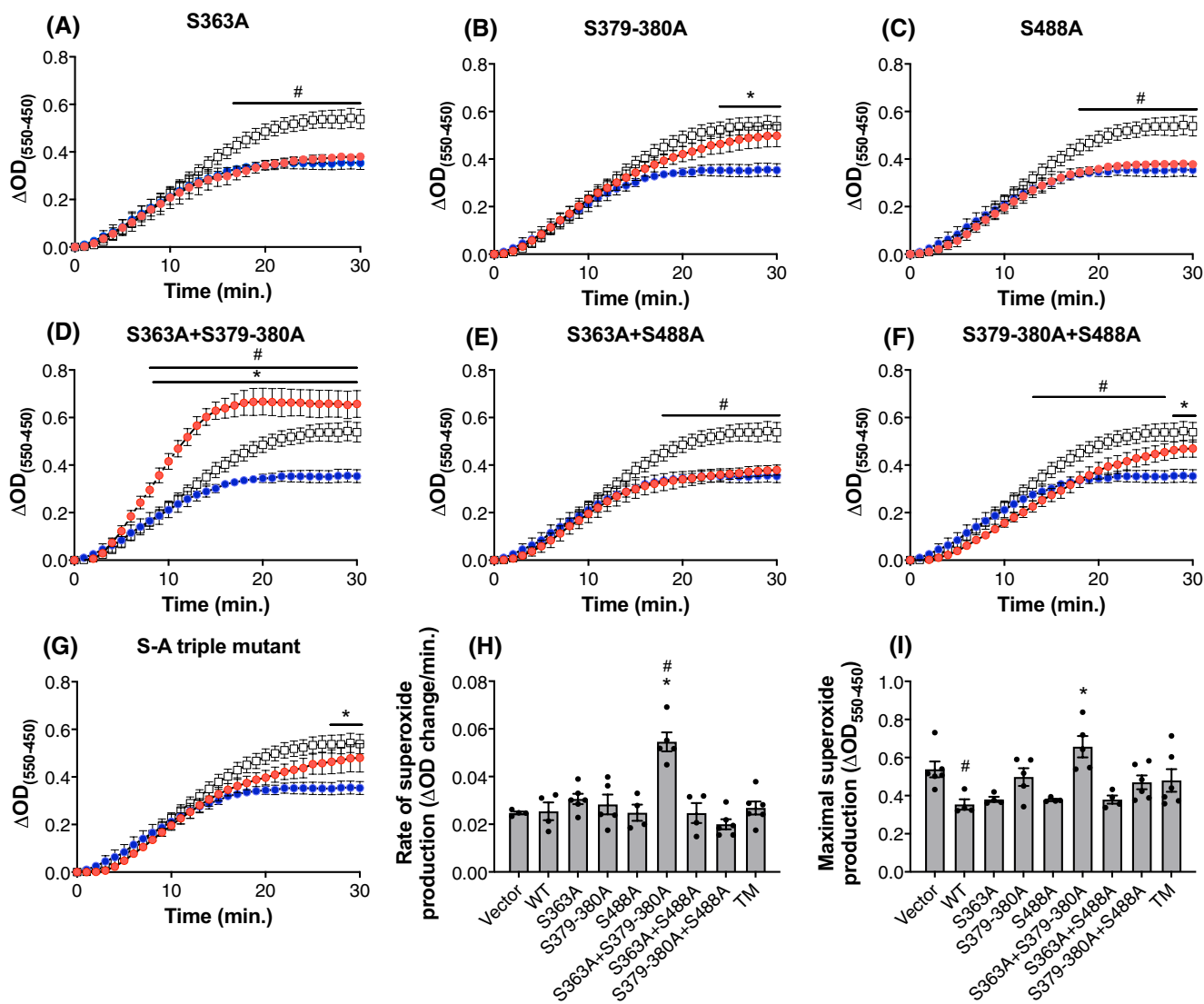
FIGURE 7 Extracellular superoxide production of PLB-985 cells transfected with different ARHGAP25 S-A mutant constructs. (A–G) PLB-985 cells were transfected with the indicated ARHGAP25 constructs and differentiated into neutrophils. Extracellular superoxide production was measured for 30 min after stimulation with 100 nM PMA by cytochrome c reduction assay; (H) The rate of superoxide production was calculated by the change of OD between minutes 4 and 10 and normalized to 1 min. (I) We determined the maximal ΔOD values and plotted them for each mutant, representing the maximal superoxide production. Mean ± SEM of four (WT, S363A, S488A, S363A + S488A) or five (Vector, S379-380A, S363A + S379-380A, S379-380A + S488A, TM) independent experiments were plotted. The lines above the diagrams show the significance of a from-to-interval. Data were analyzed using two-way ANOVA followed by a Tukey post hoc test (A–G) or one-way ANOVA (H and I). [#]$p < .05$ compared to vector. *$p < .05$ compared to WT.

After stimulation of extracellular superoxide production with PMA, S-A mutation of S363, S488 and the combination of these mutations did not alter the inhibitory effect of ARHGAP25, and superoxide production reached saturation after 20 min (Figure 7A,C,E). However, in S379-380A mutant-expressing cells, superoxide production did not reach saturation and was significantly higher than in cells transfected with wild type protein (Figure 7B). The combination of S488A with S379-380A showed a similar phenotype as S379-380A alone, suggesting that phosphorylation of S488 had no additional effect on the regulation

of superoxide production (Figure 7F). Double mutation of S363 and S379-380 to alanine not only abolished the inhibitory effect of WT on superoxide production but even increased it compared to the control vector (Figure 7D). S379-380 most probably regulates superoxide production through altering molecular interactions rather than RAC activity, thereby reversing the superoxide production decreasing effect of the wild type protein. In combination with S363A, this phenomenon could lead to the observed, rather unpredicted phenotype. The triple mutant could not increase the superoxide production but resulted in a
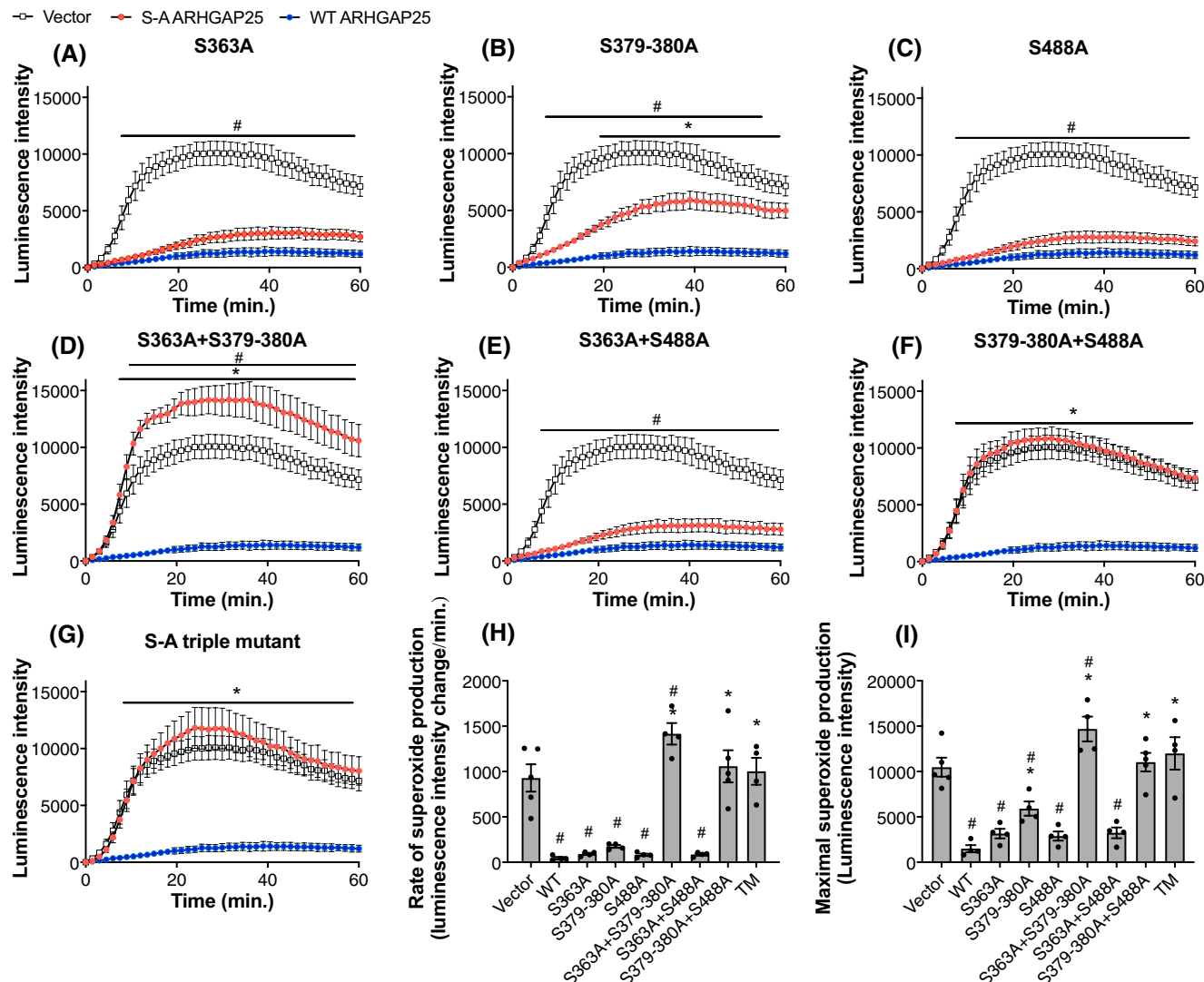
FIGURE 8 Intracellular superoxide production of PLB-985 cells transfected with different ARHGAP25 S-A mutant constructs. (A–G) PLB-985 cells were transfected with the indicated ARHGAP25 constructs and differentiated into neutrophils. Intracellular superoxide production was measured for 1 h by following lucigenin luminescence after stimulation using 1.5 mg/ml zymosan opsonized with pooled human serum; (H) The rate of superoxide production was calculated by the change of luminescence intensity between minutes 4 and 10 and normalized to 1 min. (I) We determined the maximal luminescence intensity values and plotted them for each mutant, representing the maximal superoxide production. Mean ± SEM of four independent experiments were plotted. The lines above the diagrams show the significance in a from-to-interval. Data were analyzed using two-way ANOVA followed by a Tukey post hoc test (A–G) or paired t-test (H). [#]$p < .05$ compared to vector. [*]$p < .05$ compared to WT.

similar change as we observed with S379-380A + S488A (Figure 7G). We also calculated the rate of superoxide production during 1 min as the difference of ΔOD (OD_{550}-OD_{450}) at the 10th minute minus ΔOD at the 4th minute and normalized it to 1 min (Figure 7H). These time points correspond to the linear part of the saturation curve of superoxide production. In this respect, we found that the S363A + S379-380A double mutant was the only one that differed significantly from the WT and control vector (Figure 7H). We determined the maximal ΔOD values, and again, we found a significant difference between WT and S363A + S379-380A (Figure 7I).

Next, we analyzed the intracellular superoxide production, using pooled serum opsonized zymosan (OPZ) as a more physiological stimulus. In general, data obtained with OPZ corroborated our findings on extracellular superoxide production with PMA. Mutations targeting S363 and/or S488 did not significantly decrease the inhibitory effect of ARHGAP25 (Figure 8A,C,E). S379-380A mutation alone showed a reduced superoxide-inhibitory effect, (Figure 8B) and in combination with S488A, the superoxide-inhibitory effect of WT was abolished entirely (Figure 8F,G). Once again, double mutation of S363 and S379-380 even increased the superoxide production of PLB-985 cells compared to the

control vector-transfected cells (Figure 8D). Regarding the rate of superoxide production (Figure 8H) and maximal superoxide production (Figure 8I), double mutants carrying the S379-380A mutation, and the triple mutant completely lacked their superoxide-inhibitory effect. Altogether, these data show that S379-380 has a critical role in regulating superoxide production.

4 | DISCUSSION

ARHGAP25 was previously considered a leukocyte-specific RACGAP which plays a complex role in regulating leukocyte functions, such as phagocytosis, superoxide production, and transmigration.[14–16,28] Recently, the role of ARHGAP25 in tumor cell metastasis has also been recognized.[18–23] Despite its emerging immunological and oncological importance, the post-translational control of ARHGAP25 is almost entirely unknown, prompting us to explore the regulation of this protein further.

We demonstrated in a previous study that ARHGAP25 is phosphorylated in its interdomain region[17] and that phosphorylation of serine 363 regulates the GAP activity of ARHGAP25 and thereby modulates the mobilization of hematopoietic stem cells and progenitor cells (HSPCs) from murine bone marrow.[17] Now, detailed mass spectrometry (MS) analysis confirmed the previously detected phosphorylation sites and revealed additional residues in the same region of the protein. The new MS experiments with the previous observations together suggested that S379-380 and S488 may be functionally relevant bona fide phosphorylation sites, therefore we systematically studied the role of these residues on ARHGAP25's function in the present work.

To monitor the GAP activity of ARHGAP25 in a manner that is less labor intensive and provides higher temporal resolution than currently available techniques, we first developed an in vitro, bioluminescence resonance energy transfer (BRET)-based GAP assay. In our method, the luciferase-tagged CRIB domain binds and excites exclusively the active form of RAC so we can infer the active RAC amount (and its fluctuations) from the emission (BRET) ratio. Advantages of this technique compared to other widely used methods, such as radioisotope-based GAP-assay or GTPase-Glo™ Assay are: (i) 96-well plates provide a higher number of samples and parallel experiments with every run; (ii) radioisotope labeling is not needed rendering the method safer and more cost-effective; (iii) close- to real-time temporal resolution is achievable. We verified that the BRET-based method has comparable sensitivity to other established GAP assays and still provides low variability. Moreover, our method has the potential to be adapted to monitoring guanine nucleotide exchange factor (GEF) activity.

After the verification of our BRET-GAP assay, we applied it to confirm that S363 indeed regulates the GAP activity of ARHGAP25. Additionally, we revealed that serine residue at position 488 also has a significant impact on the RACGAP activity of ARHGAP25; phosphorylation of these serine residues inhibits the in vitro RACGAP activity of ARHGAP25. Importantly, RACGAP activity proved to be independent of phosphorylation at S379-380, implying that modification at distinct residues may have specific effect on ARHGAP25 protein function. This notion was further strengthened by the observation showing that, as opposed to phosphorylation on S363A or S488A, phosphorylation of the S363A + S379-380A + S488A triple mutant ARHGAP25 with neutrophilic cytosol *decreased* its RACGAP activity.

In order to verify the observations obtained with the novel in vitro BRET assay, we performed pull-down assays to measure the amount of active RAC in resting and OPZ-stimulated neutrophilic PLB-985 cells. These experiments corroborated our BRET findings as the S363A and S488A mutants, but not the S379-380A, showed decreased RAC activity upon stimulation compared to WT (Figure S7). These data together support a hypothesis in which phosphorylation of ARHGAP25 during OPZ-evoked cell activation weakens its GAP activity resulting in more active RAC compared to the unstimulated cells. If ARHGAP25 is unable to be phosphorylated on S363 or S488, it acts as a more effective GAP.

Both active RAC and ARHGAP25 exert their biological functions near the plasmalemma. Accordingly, both proteins localize near the plasma membrane.[1–7,32] ARHGAP25's membrane-binding capacity decreases only after mutating all three serine residues (i.e., S363, S379-380, S488). Although the actual 3D structure of the protein is unknown, these residues may in fact be located relatively close to each other, and phosphorylation can cause a negatively charged area which then modifies the protein–protein interactions (e.g., the connection between ARHGAP25 and RAC), the structure, or even intramolecular interactions of ARHGAP25. This speculation is supported by the decreased plasma membrane-binding capability of the triple mutant. A similar mechanism was described for p190RhoGAP in which the phosphorylation of the polybasic region altered the protein's small GTPase specificity and membrane binding.[33]

Since ARHGAP25 is highly expressed in leukocytes and regulates their major effector responses,[14] phosphorylation of this GAP may be involved in these processes. To test this assumption, we investigated superoxide production and phagocytosis in PLB-985 cells differentiated into neutrophilic granulocytes. To induce superoxide production, we chose two widely used yet distinct stimuli: direct activation of protein kinase C (PKC) with PMA[14,16,24] or the more physiological stimulus with

TABLE 1 Summary of the effect of phosphorylation and ARHGAP25's serine-mutations on in vitro GTPase activating effect and in vivo cellular responses[a]

In vitro		In vivo			
GAP activity after phosphorylation	Mutations of ARHGAP25	Superoxide production[a]	PM localization[a]	F-Actin level[a]	Phagocytosis[a]
↓	WT				
–	S363A	–	–	–	–
↓	S379A-S380A	↑	–	–	–
–	S488A	–	–	–	–
↓	S363A + S379A-S380A	↑↑	–	↑	↓
–	S363A + S488A	–	–	–	–
–	S379A-S380A + S488A	↑	–	–	–
↓	S-A triple mutant	↑	↓	–	–

Abbreviation: PM, plasma membrane.

[a]In vivo alterations are shown compared to WT.

opsonized zymosan.[14,34] Although phosphorylation of serine residues 363 and 488 had a clear inhibitory effect on ARHGAP25's GAP activity as measured by the in vitro BRET assay, mutation of these residues did not alter superoxide production in PLB-985 neutrophilic cells. In contrast, phosphorylation of serine residues 379 and 380, which did not affect GAP activity in vitro, was required for ARHGAP25's inhibitory effect on superoxide production. Thus, ARHGAP25's GAP activity and its modulatory action on superoxide production are distinct effector functions of this protein and display highly selective sensitivity to phosphorylation.

The clear dissociation of ARHGAP25's GAP activity and its influence on superoxide production raises the possibility that the S379-380A mutant may alter the molecular interactions in the NADPH oxidase complex, rather than affecting RAC's GTPase activity itself. Our research group previously demonstrated examples of these intermolecular interactions.[16] These data suggest that phosphorylation of ARHGAP25 could regulate not only the GTPase activity of RAC but—in a steric manner—the interaction between RAC and p67^{phox} (and maybe other GAPs, e.g., p50RhoGAP) simultaneously.

Intriguingly, the S363A + S379-380A mutant displayed unexpected behavior. This mutant not only loses its inhibitory effect on superoxide production but even *increases* superoxide production when compared to vector-transfected cells. The unusual behavior of this mutant may be explained by a dominant-negative effect. However, our co-immunoprecipitation data show an impaired ARHGAP25-p50RhoGAP interaction of this double mutant (data not shown). This raises the possibility that p50RhoGAP can be excluded from the NADPH-oxidase complex, resulting in more active RAC and greatly elevated superoxide production.

When we investigated phagocytosis, a typically actin-dependent cellular response, the above-mentioned S363A + S379-380A mutant significantly decreased the ratio of phagocytosing cells which observation is opposite to its effect on the F-actin amount. As previously described, ARHGAP25 regulates not only the amount of filamentary actin but, more importantly, actin-depolymerization, and the latter is spatially critical at the cytoplasmic side of the forming phagosome during the engulfment of large particles.[28,32] Therefore, we speculate that the S363A + S379-380A mutant most likely inhibits actin-depolymerization specifically, thereby down-regulating phagocytosis. This could also explain the higher filamentary actin amount and superoxide production since the latter is known to be increased by actin-depolymerization inhibitors (e.g., cytochalasin B).[35]

5 | CONCLUSIONS

Taken together, our data indicate that the RACGAP activity of ARHGAP25 is regulated directly by the phosphorylation of serine residues at positions 363 and/or 488, but not at 379–380, in vitro. In live cells, S363 and S379-380 together regulate superoxide production and phagocytosis, most probably through parallel modulation of RACGAP activity and actin-depolymerization (Table 1). We speculate that distinct phosphorylation patterns of ARHGAP25 result in specific functional states of this protein, similar to that described for heterotrimeric G-proteins ("barcode-dependent regulation").[36,37]

AUTHOR CONTRIBUTIONS

Éva Wisniewski developed the methodology; Éva Wisniewski and Domonkos Czárán carried out the formal analysis and investigation and wrote the original

DISCLOSURES
The authors declare no conflict of interest.

DATA AVAILABILITY STATEMENT
Raw mass spectrometry data and a summary Excel file are openly available in figshare at https://doi.org/10.6084/m9.figshare.19221312.

ORCID
Roland Csépányi-Kömi https://orcid.org/0000-0001-6825-7142

REFERENCES
1. Burridge K, Wennerberg K. Rho and Rac take center stage. *Cell*. 2004;116:167-179.
2. Jaffe AB, Hall A. Rho GTPases: biochemistry and biology. *Annu Rev Cell Dev Biol*. 2005;21:247-269.
3. Heasman SJ, Ridley AJ. Mammalian rho GTPases: new insights into their functions from in vivo studies. *Nat Rev Mol Cell Biol*. 2008;9:690-701.
4. Parsons JT, Horwitz AR, Schwartz MA. Cell adhesion: integrating cytoskeletal dynamics and cellular tension. *Nat Rev Mol Cell Biol*. 2010;11:633-643.
5. Hall A. Rho family GTPases. *Biochem Soc Trans*. 2012;40:1378-1382.
6. Sadok A, Marshall CJ. Rho GTPases: masters of cell migration. *Small GTPases*. 2014;5:e29710.
7. Bokoch GM. Regulation of innate immunity by rho GTPases. *Trends Cell Biol*. 2005;15:163-171.
8. Bos JL, Rehmann H, Wittinghofer A. GEFs and GAPs: critical elements in the control of small G proteins. *Cell*. 2007;129:865-877.
9. McCormack J, Welsh NJ, Braga VM. Cycling around cell-cell adhesion with rho GTPase regulators. *J Cell Sci*. 2013;126:379-391.
10. Cook DR, Rossman KL, Der CJ. Rho guanine nucleotide exchange factors: regulators of rho GTPase activity in development and disease. *Oncogene*. 2014;33:4021-4035.
11. van Buul JD, Geerts D, Huveneers S. Rho GAPs and GEFs: controling switches in endothelial cell adhesion. *Cell Adh Migr*. 2014;8:108-124.
12. Boguski MS, McCormick F. Proteins regulating Ras and its relatives. *Nature*. 1993;366:643-654.
13. Katoh M, Katoh M. Identification and characterization of ARHGAP24 and ARHGAP25 genes in silico. *Int J Mol Med*. 2004;14:333-338.
14. Csépányi-Kömi R, Sirokmány G, Geiszt M, Ligeti E. ARHGAP25, a novel Rac GTPase-activating protein, regulates phagocytosis in human neutrophilic granulocytes. *Blood*. 2012;119:573-582.
15. Csépányi-Kömi R, Wisniewski É, Bartos B, et al. Rac GTPase activating protein ARHGAP25 regulates leukocyte Transendothelial migration in mice. *J Immunol*. 2016;197:2807-2815.
16. Lőrincz ÁM, Szarvas G, Smith SM, Ligeti E. Role of Rac GTPase activating proteins in regulation of NADPH oxidase in human neutrophils. *Free Radic Biol Med*. 2014;68:65-71.
17. Wang LD, Ficarro SB, Hutchinson JN, et al. Phosphoproteomic profiling of mouse primary HSPCs reveals new regulators of HSPC mobilization. *Blood*. 2016;128:1465-1474.
18. Thuault S, Comunale F, Hasna J, et al. The RhoE/ROCK/ARHGAP25 signaling pathway controls cell invasion by inhibition of Rac activity. *Mol Biol Cell*. 2016;27:2653-2661.
19. Tao L, Gu Y, Zheng J, Yang J, Zhu Y. Weichang'an suppressed migration and invasion of HCT116 cells by inhibiting Wnt/β-catenin pathway while upregulating ARHGAP25. *Biotechnol Appl Biochem*. 2019;66:787-793.
20. Tao L, Zhu Y, Gu Y, Zheng J, Yang J. ARHGAP25: a negative regulator of colorectal cancer (CRC) metastasis via the Wnt/β-catenin pathway. *Eur J Pharmacol*. 2019;858:172476.
21. Xu K, Liu B, Ma Y. The tumor suppressive roles of ARHGAP25 in lung cancer cells. *Onco Targets Ther*. 2019;12:6699-6710.
22. Huang WK, Chen Y, Su H, et al. ARHGAP25 inhibits pancreatic adenocarcinoma growth by suppressing glycolysis via AKT/mTOR pathway. *Int J Biol Sci*. 2021;17:1808-1820.

23. Ding FP, Tian JY, Wu J, Han DF, Zhao D. Identification of key genes as predictive biomarkers for osteosarcoma metastasis using translational bioinformatics. *Cancer Cell Int*. 2021;21: 640.

24. Rada BK, Geiszt M, Káldi K, Timár C, Ligeti E. Dual role of phagocytic NADPH oxidase in bacterial killing. *Blood*. 2004;104:2947-2953.

25. Kobayashi K, Suzuki T, Iwata E, et al. Transcriptional repression by MYB3R proteins regulates plant organ growth. *EMBO J*. 2015;34:1992-2007.

26. Hubner NC, Bird AW, Cox J, et al. Quantitative proteomics combined with BAC TransgeneOmics reveals in vivo protein interactions. *J Cell Biol*. 2010;189:739-754.

27. Klement E, Gyula P, Viczián A. Detection of phytochrome phosphorylation in plants. *Methods Mol Biol*. 2019;2026:41-67.

28. Schlam D, Bagshaw RD, Freeman SA, et al. Phosphoinositide 3-kinase enables phagocytosis of large particles by terminating Actin assembly through Rac/Cdc42 GTPase-activating proteins. *Nat Commun*. 2015;6:8623.

29. Nomura M, He Z, Koyama I, Ma WY, Miyamoto K, Dong Z. Involvement of the Akt/mTOR pathway on EGF-induced cell transformation. *Mol Carcinog*. 2003;38:25-32.

30. Ridley AJ, Paterson HF, Johnston CL, Diekmann D, Hall A. The small GTP-binding protein rac regulates growth factor-induced membrane ruffling. *Cell*. 1992;70:401-410.

31. Csépányi-Kömi R, Sáfár D, Grósz V, Tarján ZL, Ligeti E. In silico tissue-distribution of human rho family GTPase activating proteins. *Small GTPases*. 2013;4:90-101.

32. Csépányi-Kömi R, Pásztor M, Bartos B, Ligeti E. The neglected terminators: rho family GAPs in neutrophils. *Eur J Clin Invest*. 2018;48(Suppl 2):e12993.

33. Lévay M, Settleman J, Ligeti E. Regulation of the substrate preference of p190RhoGAP by protein kinase C-mediated phosphorylation of a phospholipid binding site. *Biochemistry*. 2009;48:8615-8623.

34. Cohen HJ, Newburger PE, Chovaniec ME, Whitin JC, Simons ER. Opsonized zymosan-stimulated granulocytes-activation and activity of the superoxide-generating system and membrane potential changes. *Blood*. 1981;58:975-982.

35. Becker EL, Sigman M, Oliver JM. Superoxide production induced in rabbit polymorphonuclear leukocytes by synthetic chemotactic peptides and A23187. *Am J Pathol*. 1979; 95:81-97.

36. Flock T, Hauser AS, Lund N, Gloriam DE, Balaji S, Babu MM. Selectivity determinants of GPCR-G-protein binding. *Nature*. 2017;545:317-322.

37. Kaya AI, Perry NA, Gurevich VV, Iverson TM. Phosphorylation barcode-dependent signal bias of the dopamine D1 receptor. *Proc Natl Acad Sci U S A*. 2020;117:14139-14149.

SUPPORTING INFORMATION

Additional supporting information can be found online in the Supporting Information section at the end of this article.